ACS Photonics

Article

pubs.acs.org/journal/apchd5

Visible Spectrum Quantum Light Sources Based on $In_xGa_{1-x}N$/GaN Quantum Dots

Stanko Tomić,*,† Joydeep Pal,‡ Max A. Migliorato,‡ Robert J. Young,§ and Nenad Vukmirović‖

†Joule Physics Laboratory, School of Computing Science and Engineering, University of Salford, Manchester M5 4WT, United Kingdom

‡School of Electrical and Electronic Engineering, University of Manchester, Manchester M13 9PL, United Kingdom

§Department of Physics, Lancaster University, Lancaster LA1 4YB, United Kingdom

‖Scientific Computing Laboratory, Institute of Physics Belgrade, University of Belgrade, Pregrevica 118, 11080 Belgrade, Serbia

Supporting Information

ABSTRACT: We present a method for designing quantum light sources, emitting in the visible band, using wurtzite $In_xGa_{1-x}N$ quantum dots (QDs) in a GaN matrix. This system is significantly more versatile than previously proposed arsenide- and phosphide-based QDs, having a tuning range exceeding 1 eV. The quantum mechanical configuration interaction method, capturing the fermionic nature of electrons and associated quantum effects explicitly, is used to find shapes and compositions of dots to maximize the excitonic dipole matrix element and optimize the biexciton binding energy. These results provide QD morphologies tailored for either bright single-photon emission or entangled-photon-pair emission at any given wavelength in the visible spectrum.

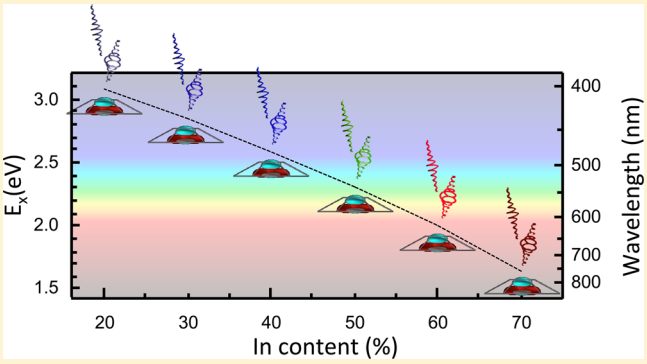

KEYWORDS: *single-photon sources, entanglement, quantum dots, correlations, III-nitrides, inverse problems*

The breakthrough in the development of solid-state lighting was recently recognized by the Nobel Prize in Physics 2014 awarded to Isamu Akasaki, Hiroshi Amano, and Shuji Nakamura.[1] It is important to build upon this work and develop practical and versatile sources of quantum light because they are key components required for the advancement of quantum photonic devices. Proof-of-principle demonstrations with InAs/GaAs,[2,3] GaN/AlN,[4] and phosphide-compatible[6,7] material systems have shown that solid-state quantum dots (QDs) can be near-ideal sources of quantum light, albeit covering narrow wavelength ranges. There are many applications of quantum light beyond quantum communications at telecoms wavelengths, such as beating the classical diffraction limit in quantum imaging[8] or reducing cell damage in the microscopy of biological systems.[9] QD light sources have already been used to exceed classical optical interferometry limits,[10] but the long wavelength of emission from the InAs QDs used in this demonstration severely limited its appeal.

Radiative recombination from excitons confined in InGaN/GaN wurtzite QDs could provide versatility not afforded by other material systems, helping to target new applications of quantum photonics. Excitons in nitride quantum dots have large emission energies, unlocking the blue and ultraviolet spectral regions for quantum light sources (QLS) that have been inaccessible to common III−V zinc-blende compatible technologies. Stronger quantum-confinement effects, resulting from their large band gaps, band offsets, and effective masses also make wurtzite nitride-based QLS suitable for operating at higher temperatures.[4,5] Recent experiments have also reported the bound biexcitons in small III-N-based QDs.[11−13] In comparison to GaN/AlN QDs,[4,14,15] the use of $In_xGa_{1-x}N$ in GaN host lattice results in longer emission wavelengths, with the modulation of the indium content providing an additional degree of freedom required to tune the emission wavelength of photon sources throughout the visible spectral band. Also, previous reports of InGaN single-QD-based spectroscopy experiments[16−18] show improved photon correlations and extraction efficiency.[19−22] This is particularly important in applications requiring cheap, high-performance single-photon detectors such as visible and free-space high-bandwidth quantum communications because InGaN/GaN QDs can offer compatibility with silicon-based avalanche photodiodes.[23]

To design the nanofabrication of QDs to meet the demands of specific applications, a relationship between morphology and the confined excitonic states needs to be found. This is challenging because of the effects of strain, band mixing, quantum confinement, Coulomb interactions, and correlations

Received: March 28, 2015
Published: June 9, 2015

 © 2015 American Chemical Society

DOI: 10.1021/acsphotonics.5b00159
ACS Photonics 2015, 2, 958−963

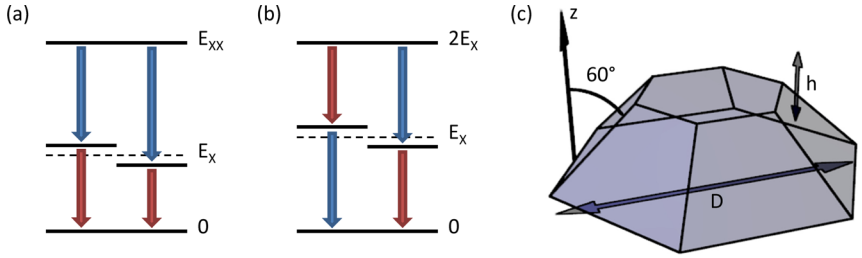

Figure 1. Simple energy level diagrams depicting the two-photon biexciton (XX) cascade through the bright intermediate exciton (X) states with (a) a large biexciton shift, allowing photons from the biexciton and exciton states to be easily separated, and (b) zero binding energy, a condition allowing entangled-photon generation through time reordering. (c) Illustration depicting the hexagonal-based geometry of the quantum dot used in our calculations.

among particles present in the QD system. Furthermore, particle confinement in wurtzite QDs is strongly affected by large built-in electric fields induced by both spontaneous, linear and nonlinear piezoelectric polarizations.[24] Here, we establish such a relationship using the configuration interaction (CI) method, showing that emission from InGaN/GaN QDs can be optimized for both single- and entangled-photon emission throughout the visible spectrum.

The optimal QLS parameters differ depending on the type of light source required, as illustrated in Figure 1a,b. For single-photon sources it is desirable to maximize the biexciton (XX) shift so that in the two-photon cascade through the intermediate exciton (X) state the two photons have a large spectral separation[4] as shown in Figure 1a. Successful spectral separation of the two photons always requires an optical component, but in practice, its ease of implementation is dependent on the energetic separation of the exciton and biexciton photons. At the limit of large separation an efficient, low-cost cold mirror can be employed, whereas differentiation below <1 meV requires expensive impractical filtering.[3] The former minimizes the resources required to select emission from a single excitonic state because the required precision in the wavelength-dependent optics reduces with increasing energy separation between the biexciton and exciton photons. In contrast, entangled photons can be generated through time reordering when the biexciton shift is zero,[25] as depicted in Figure 1b. We want to point out that we are not considering here an entangled-photon sources scheme that is based on the vanishing fine structure splitting, $FSS = 0$, already realized and elaborated in the literature.[3,26,27] We focus our analysis to the time-reordering scheme to generate entangled-photon pairs that requires $B_{XX} = 0$.[28,29]

The biexciton shift can be expressed as $B_{XX} = (E_{XX} - E_X) - E_X$, where E_{XX} is the energy of the biexciton in its ground state and E_X is the average energy of the two intermediate bright exciton states. In this material system, it has been shown that the internal electric field localizes the electrons at the top and the holes at the bottom of the dot.[30] As a consequence of this charge separation, the repulsive e − e and h − h Coulomb interactions rapidly dominate as the dot height increases, leading to an increase in the biexciton shift.[11,15] As the electron and hole separation increases, however, the optical transition matrix element for exciton recombination, p_X, decreases, undesirably reducing the maximum repetition rate of the photon source.[31] Thus, the two requirements for an ideal single-photon source, i.e., maximum intensity and spectral purity, have competing demands on the dot's height. We express this conflict in an optimization function Ξ that can be used to find the best balance between the requirements; it is defined as follows:[15,32]

$$\Xi = (E_{XX} - 2E_X)\ln\left(\frac{p_X^{(x)}}{p_X^{(0)}}\right) \tag{1}$$

where $p_X^{(x)}$ is the value of the x component of the dipole matrix element of the exciton transition, $p_X^{(0)}$ is equal to $10^{-4}p_X^{(x),\max}$, and $p_X^{(x),\max}$ is the maximal value of $p_X^{(x)}$ for all quantum dots considered. Although the choice of $p_X^{(0)}$ is somewhat arbitrary, we find that the position of the maxima of the optimization function are weakly dependent on its value when it is changed within reasonable limits. Within the range of energies in which the optimization function, eq 1, is studied, the maximum biexciton shift remains within the small limit, i.e., within an order of magnitude of the typical line width of emission.[3] In this limit the assumption discussed earlier, i.e., that larger shifts are advantageous for efficient cheap filtering, holds true.

In our theoretical model, the single-particle electron and hole states of wurtzite $In_xGa_{1-x}N$/GaN QDs were modeled using the eight-band **k·p** Hamiltonian,[15,33,34] consisting of the kinetic part that includes spin−orbit interaction, the crystal-field splitting, the strain part, and additional terms arising from the presence of spontaneous and piezoelectric polarization. The strain, spontaneous, and piezo field were relaxed on augmented embedding box until convergency in several lowest electron (e) and highest hole (h) states was achieved.[15] After the single-particle states were found, the (bi)exciton states were obtained using the CI method,[15,35] i.e., by direct diagonalization of the CI Hamiltonian. The many-body CI Hamiltonian contains only particle-conserving terms and is given by

$$H = \sum_i^{N_e} E_i \hat{e}_i^\dagger \hat{e}_i - \sum_i^{N_h} E_i \hat{h}_i^\dagger \hat{h}_i + \frac{1}{2}\sum_{ijkl}^{N_e} V_{iljk}\hat{e}_i^\dagger \hat{e}_j^\dagger \hat{e}_k \hat{e}_l + \frac{1}{2}\sum_{ijkl}^{N_h} V_{iljk}\hat{h}_i^\dagger \hat{h}_j^\dagger \hat{h}_k \hat{h}_l - \sum_{ijkl}^{N_e,N_h} (V_{iljk} - V_{ikjl})\hat{e}_i^\dagger \hat{h}_j^\dagger \hat{h}_k \hat{e}_l \tag{2}$$

To get excitonic states, we write the Hamiltonian, eq 2, in a two-particle basis (one electron and one hole) $|i, j\rangle = |e_i\rangle\ |h_j\rangle$, and for biexcitons, we use a four-particle basis $|i,j,k,l\rangle = |e_i\rangle\ |h_j\rangle\ |e_k\rangle\ |h_l\rangle$.[36] Coulomb integrals, V_{ijkl}, required for the diagonalization of the CI Hamiltonian were evaluated in reciprocal space and then corrected using the Makov-Payne method[37] adapted for a hexagonal lattice[15] by adding the first few terms (monopole, dipole, and quadrupole) in the multipole expansion to compensate for the effect of the mirror charges induced by periodic boundary conditions. In this way, the model faithfully

DOI: 10.1021/acsphotonics.5b00159
ACS Photonics 2015, 2, 958−963

represents electronic and excitonic structure of a single QD.[15] All calculations presented here are performed with kppw parallel code.[38]

In our analysis of single InGaN/GaN QDs, we have assumed a hexagonal truncated-pyramidal shape, most often used in the analysis of other wurtzite QD, e.g., GaN/AlN QD. Although InGaN QDs grown on the top of quantum wire (QWR) exhibit quite regular form, it is worth pointing out that the actual shape of InGaN QDs is still unclear and could differ from the perfectly symmetric one; the choice of shape here should be considered as an approximation to the real one. A model QD, in the shape of a hexagonal truncated pyramid is illustrated in Figure 1c. It is assumed that the QD is positioned on a wetting layer (WL) that is 0.5185 nm thick. The dimensions of the QD are controlled by two independent parameters: the diameter, D, of the circumscribed circle around the hexagon at the WL−QD interface at $z = 0$, and the angle between pyramid base and pyramid side edges, which is assumed to be $\alpha = 30°$. The size of the QDs was controlled by D/h aspect ratio, where h is the QD height. The calculations are performed over a wide range of QDs with In content ranging from 10 to 80%. All the CI calculations involved single-particle electron ($N_e = 12$) and hole ($N_h = 18$) states, including both spins.

As a first step in our optimization, we calculate the biexciton shift of a variety of InGaN/GaN QD structures, therefore assessing its qualification as a QLS. One of the major shortcomings of the mean-field theories, such as Hartree or Hartree−Fock approaches, is the lack of electron correlation effects, whereas the CI approach is capable of capturing such quantum effects explicitly. This is of paramount importance in small QDs, where the direct Coulomb integrals can be comparable in energy to the correlation effect. For a series of smaller $In_xGa_{1-x}N$/GaN QDs, we have calculated the excitonic and biexcitonic states with In content varying from 10 to 80% and changing the QD heights in the range of $h = 1-2.1$ nm with 0.1 nm steps, as shown in Figure 2. The crossover between unbound to bound biexcitonic states is observed for all In compositions greater than or equal to 20% and for the aspect ratios $D/h = 4$, 5, 6, and 7. As the In content reduces, the QD confinement potential for electrons and holes diminishes, leading in turn to a reduction in the number of confined states. This limits the effect of correlations, which eventually (In $x <$ 20%) prevents the formation of bound biexciton.

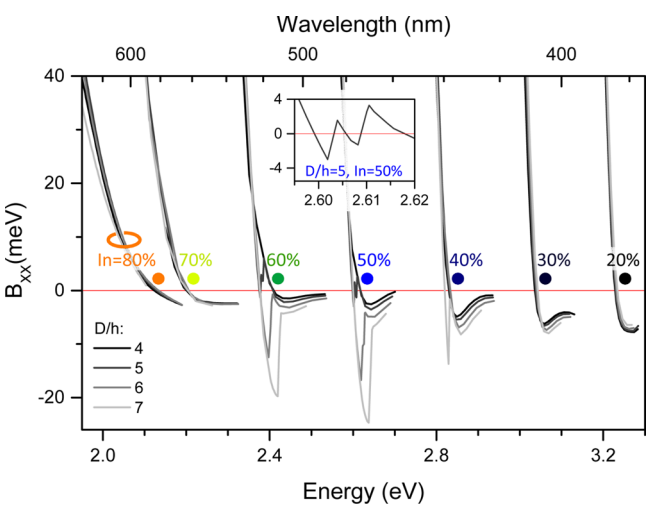

Figure 2. Biexciton binding energy as a function of the exciton's emission energy for different indium concentrations in the quantum dot and diameter/height (D/h) ratios as labeled. Colored circles roughly indicate the wavelength of emission at zero binding energy for each indium composition. Inset highlights the case for $D/h = 5$ and 50% indium composition, showing five energies at which the biexciton shift crosses zero.

By analyzing the results presented in Figure 2, several observations regarding the excitonic structure of $In_xGa_{1-x}N$/GaN single QDs can be made: (1) By varying the aspect ratio (D/h) and height h, i.e., QD dimensions, for each In composition greater than or equal to 20%, it was possible to identify the range of excitonic energies at which transition from unbound to bound biexciton occurs, i.e., $B_{XX} = 0$. This is important because such morphologies are suitable to fulfill the criteria for the operation of entangled-photon sources. (2) By moving from smaller (right side of the traces) to larger QDs (left side of the traces), it can be observed that smaller QDs support bound biexcitons, whereas large ones do not. Small QDs produce less strain because of smaller volume and, consequently, the smaller piezoelectric field around them, with less ability to reduce the overlap between electron and hole wave function. Good overlap between wave functions produces strong correlation that in turn makes the biexciton bound. With increasing QD size, more states can be confined, contributing more toward correlation, and we observe characteristic minima in B_{XX} for certain QD sizes and for In content between 30 and 60%. For large QDs, the piezoelectric field becomes so strong that the overlap of wave functions is strongly reduced, and in this way, the correlation effect is reduced as well. In such QDs, the correlation effect is no longer strong enough to overcome the e − e and h − h repulsive interactions in a biexciton, leading to its unbound character. In Figure 4, the top line shows the exciton emission energy and indium contents that satisfy the $B_{XX} = 0$ condition. (3) For certain aspect ratios from the $D/h =$ 5, 6, and 7 range and In contents of 40−50%, we observe a sudden drop in B_{XX} and strongly bound biexcitons. This phenomenon arises from the confinement of increased number of states (particularly in *VB* where h states exhibit much larger density of states because of larger effective masses) with a small variation in QD dimensions that lead to increased correlations. However, for QDs with large In content (70%), the effect of internal electric field dominates and destroys the conditions for strong correlations as explained in item 2. In QDs with smaller In content of 20 and 30%, such effect is not observed because of two reasons: (a) Such QDs exhibit shallower confinement with much less bound states capable of contributing to correlations. (b) A smaller amount of In in a QD results in a smaller effect of an internal electric field on wave function overlap within QD structures. (4) Also, we want to highlight that for the case of 50% In content and aspect ratio $D/h = 5$ we observe five crossings between bound and unbound states over the range of 30 meV of excitonic energies from $E_X = 2.60-2.62$ eV (inset in Figure 2). This is the region with the most suitable morphology for entangled-photon source devices.

In the Supporting Information, all morphologies that exhibit $B_{XX} = 0$ in Figure 3 are listed, together with excitonic energy deviations from the excitonic energy at which $B_{XX} = 0$.

After identifying suitable In contents, we proceed now with the optimization of single QDs for single photon source (SPS) devices. For QDs with the In content in the range from 20 to 70%, the aspect ratio in the range $D/h = 6-11$, and the QD height in the range $h = 1-6$ nm, we have calculated the excitonic ground state energy, E_X, its dipole, p_X, the biexcitonic

DOI: 10.1021/acsphotonics.5b00159
ACS Photonics 2015, 2, 958−963

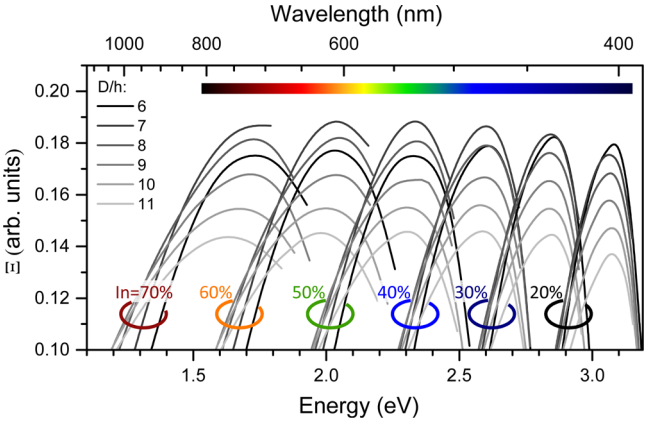

Figure 3. Dependence of the optimization function Ξ, eq 1 defined in the text, on exciton emission energy for different indium concentrations in the quantum dot and diameter/height (D/h) ratios as labeled. The colored circles roughly indicate the wavelength of emission at which Ξ is maximized for each indium composition.

energy, E_{XX}, and the optimization function, Ξ, eq 1. The results of the optimization procedure are given in Figure 3. We have observed that for each In concentration it is possible to identify a maximum in function Ξ. QD morphologies that support these maxima will provide the best SPS devices at particular wavelengths. Optimization function Ξ, eq 1, assumes only the unbound biexcitons. However, by replacing $E_{XX} - 2E_X$ with $|E_{XX} - 2E_X|$, the search can be extended to bound biexcitons as well. We have found local maxima of Ξ in that region to be negligible. In Figure 4, we plot the exciton energy (wavelength)

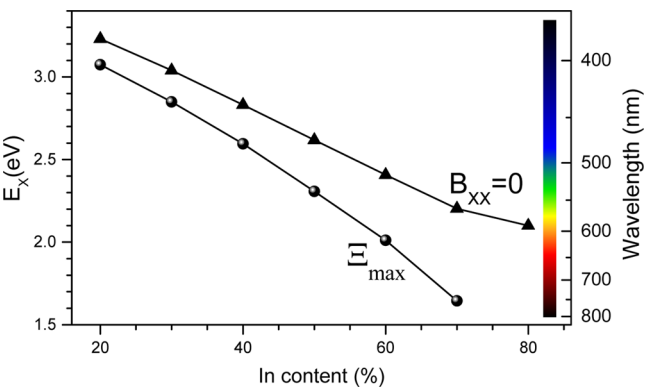

Figure 4. Exciton emission energy plotted as a function of indium composition at the point at which the optimization function (Ξ) is maximized (●) and at the points where the biexciton shift is zero (▲).

versus In concentration for the most optimal SPS QDs. The dimensions of those QDs, i.e., aspect ratio, height in nanometers, and In concentrations (%) together with the emitting wavelengths in micrometers, are (6, 2.6, 20%, 0.401), (9, 2.1, 30%, 0.439), (7, 2.2, 40%, 0.466), (7, 2.4, 50%, 0.539), (7, 2.2, 60%, 0.603), and (7, 2.2, 70%, 0.743). In contrast, for very small QDs with $D/h = 4$ and 5, B_{XX} is small so that local maxima for these aspect ratios are lower than the one for $D/h = 6$; in addition, biexcitons become bound before Ξ can reach local maxima for all In concentrations considered. In the Supporting Information, all morphologies that exhibit maxima in Figure 3 are listed, together with their emission wavelengths. From Figure 4, it is clearly seen that with suitable modulation of the In content and careful design of QD dimensions it is possible to achieve the $In_xGa_{1-x}N/GaN$ QD-based SPS emission in the range from $\lambda_{min} = 0.403$ μm to $\lambda_{max} = 0.754$ μm that covers the entire visible spectrum.

Recently, Deshpande et al.[20] realized good quality electrically injected single-photon sources that are based on InGaN quantum dots in GaN nanowires. The dots in ref 20 have a height of 2 nm and a diameter of about 25 nm. Our results indicate that optimal dot dimensions are typically slightly larger than 2 nm and therefore agree with the fact that good quality single-photon sources were realized in ref 20 with dots of similar dimensions.

In addition to the emission wavelength other factors, such as the repetition rate, the output coupling efficiency, and coherence of the emission, need to be taken into consideration in the design of SPS sources. We have estimated from the excitonic lifetime in InGaN QDs that the repetition rate of our SPS sources will be in the gigahertz range. Purcell enhancement in an optical cavity could increase this even further.[41] As-grown QDs typically have poor output coupling efficiency, which however could be rectified with structural engineering.[42] The emission from QDs can be highly coherent,[43] although many applications of quantum light do not require coherency of light. Also, it is very likely that the addition of the Al in the barrier material, i.e., InGaN/AlGaN QD system, could provide for better thermal characteristics because of larger confinement potentials for electrons and holes, leading further toward higher temperature operations.

We have shown that with suitable variation of the In/Ga ratio in single $In_xGa_{1-x}N/GaN$ QDs it is possible to tune both SPS and entangled-photon emission covering the whole visible spectrum. Using the CI method, including the effect of electron exchange and correlations interactions, we have shown that in small QDs the exchange-correlation effect is sufficient enough to compensate for the increase of the direct Coulomb energy of two excitons in a QD. Because InGaN materials have smaller piezoelectric and spontaneous polarization effects than those in GaN, the exchange-correlation effect is not capable of simultaneously reducing the electron−hole attraction (and exchange-correlation) and increasing the pairwise Coulomb repulsion. It is currently thought that InGaN QDs are formed as local composition fluctuations in quantum wells. Although it is unlikely that such structures provide the level of control over QD morphology required to optimize SPS and entangled-photon devices for planar structures, InGaN QDs formed in GaN nanowires present a promising alternative system where good SPSs have already been realized.[20,22,39,40] Our designs can serve as a guidance of further development of this technology. In combination with recent work optimizing the brightness,[41] efficiency,[42] and coherence of light from quantum dots,[43] the results presented here can be used to design light sources for a number of applications including quantum imaging and communications.

■ ASSOCIATED CONTENT

Supporting Information

Relevant information on QD morphologies required for the optimal SPSs and entangled-photon sources. The Supporting Information is available free of charge on the ACS Publications website at DOI: 10.1021/acsphotonics.5b00159.

■ AUTHOR INFORMATION

Corresponding Author

*E-mail: s.tomic@salford.ac.uk.

DOI: 10.1021/acsphotonics.5b00159
ACS Photonics 2015, 2, 958−963

Notes

The authors declare no competing financial interest.

■ ACKNOWLEDGMENTS

S.T. thanks the Royal Society, London (grant "High Performance Computing in Modelling of Innovative Photo-Voltaic Devices"), EU-COST (project MP1406), and the STFC, United Kingdom, for providing the computational resources. J.P. thanks EPSRC for a Doctoral Prize Fellowship. R.J.Y. acknowledges support by the Royal Society through a University Research Fellowship (UF110555). N.V. was supported by European Community FP7 Marie Curie Career Integration Grant (ELECTROMAT) and Serbian Ministry of Education, Science and Technological Development (project ON171017). We thank Mark Holmes for valuable suggestions and discussions.

■ REFERENCES

(1) Nobel Media AB 2014. *The Nobel Prize in Physics 2014*. http://www.nobelprize.org/nobel_prizes/physics/laureates/2014/ (accessed on January 28, 2015).

(2) Michler, P.; Kiraz, A.; Becher, C.; Schoenfeld, W. V.; Petroff, P. M.; Zhang, L. D.; Hu, E.; Imamoglu, A. A Quantum Dot Single-Photon Turnstile Device. *Science* **2000**, *290*, 2282−2285.

(3) Stevenson, R. M.; Young, R. J.; Atkinson, P.; Cooper, K.; Ritchie, D. A.; Shields, A. J. A semiconductor source of triggered entangled photon pairs. *Nature* **2006**, *439*, 179−182.

(4) Kako, S.; Santori, C.; Hoshino, K.; Gotzinger, S.; Yamamoto, Y.; Arakawa, Y. A gallium nitride single-photon source operating at 200 K. *Nat. Mater.* **2006**, *5*, 887−892.

(5) Holmes, M. J.; Choi, K.; Kako, S.; Arita, M.; Arakawa, Y. Room-Temperature Triggered Single Photon Emission from a III-Nitride Site-Controlled Nanowire Quantum Dot. *Nano Lett.* **2014**, *14*, 982−986.

(6) Benyoucef, M.; Yacob, M.; Reithmaier, J. P.; Kettler, J.; Michler, P. Telecom-wavelength (1.5 μ m) single-photon emission from InP-based quantum dots. *Appl. Phys. Lett.* **2013**, *103*, 162101.

(7) Miyazawa, T.; Takemoto, K.; Sakuma, Y.; Hirose, S.; Usuki, T.; Yokoyama, N.; Takatsu, M.; Arakawa, Y. Single-Photon Generation in the 1.55-μm Optical-Fiber Band from an InAs/InP Quantum Dot. *J. J. Appl. Phys. Lett.* **2005**, *44*, L620.

(8) Boto, N.; Kok, P.; Abrams, D. S.; Braunstein, S. L.; Williams, C. P.; Dowling, J. P. Quantum Interferometric Optical Lithography: Exploiting Entanglement to Beat the Diffraction Limit. *Phys. Rev. Lett.* **2000**, *85*, 2733−2736.

(9) Giovannetti, V.; Lloyd, S.; Maccone, L. Quantum-Enhanced Measurements: Beating the Standard Quantum Limit. *Science* **2004**, *306*, 1330−1336.

(10) Stevenson, R. M.; Hudson, A. J.; Young, R. J.; Atkinson, P.; Cooper, K.; Ritchie, D. A.; Shields, A. J. Biphoton interference with a quantum dot entangled light source. *Opt. Express* **2007**, *15*, 6507−6512.

(11) Simeonov, D.; Dussaigne, A.; Butté, R.; Grandjean, N. Complex behavior of biexcitons in GaN quantum dots due to a giant built-in polarization field. *Phys. Rev. B* **2008**, *77*, 075306.

(12) Renard, J.; Songmuang, R.; Bougerol, C.; Daudin, B.; Gayral, B. Exciton and Biexciton Luminescence from Single GaN/AlN Quantum Dots in Nanowires. *Nano Lett.* **2008**, *8*, 2092−2096.

(13) Choi, K.; Kako, S.; Holmes, M. J.; Arita, M.; Arakawa, Y. Strong exciton confinement in site-controlled GaN quantum dots embedded in nanowires. *Appl. Phys. Lett.* **2013**, *103*, 171907.

(14) Callsen, G.; Carmele, A.; Hönig, G.; Kindel, C.; Brunnmeier, J.; Wagner, M. R.; Stock, E.; Reparaz, J. S.; Schliwa, A.; Reitzenstein, S.; Knorr, A.; Hoffmann, A.; Kako, S.; Arakawa, Y. Steering photon statistics in single quantum dots: From one- to two-photon emission. *Phys. Rev. B* **2013**, *87*, 245314.

(15) Tomić, S.; Vukmirović, N. Excitonic and biexcitonic properties of single GaN quantum dots modeled by 8-band **k·p** theory and configuration-interaction method. *Phys. Rev. B* **2009**, *79*, 245330.

(16) Moriwaki, O.; Someya, T.; Tachibana, K.; Ishida, S.; Arakawa, Y. Narrow photoluminescence peaks from localized states in InGaN quantum dot structures. *Appl. Phys. Lett.* **2000**, *76*, 2361.

(17) Schömig, H.; Halm, S.; Forchel, A.; Bacher, G.; Off, J.; Scholz, F. Probing Individual Localization Centers in an InGaN/GaN Quantum Well. *Phys. Rev. Lett.* **2004**, *92*, 106802.

(18) Collins, D. P.; Jarjour, A. F.; Taylor, R. A.; Hadjipanayi, M.; Oliver, R. A.; Kappers, M. J.; Humphreys, C. J.; Tahraoui, A. Two-photon autocorrelation measurements on a single InGaN/GaN quantum dot. *Nanotechnology* **2009**, *20*, 245702.

(19) Taylor, R. A.; Jarjour, A. F.; Collins, D. P.; Holmes, M. J.; Oliver, R. A.; Kappers, M. J.; Humphreys, C.J. Cavity Enhancement of Single Quantum Dot Emission in the Blue. *Nanoscale Res. Lett.* **2010**, *5*, 608−612.

(20) Deshpande, S.; Heo, J.; Das, A.; Bhattacharya, P. Electrically driven polarized single-photon emission from an InGaN quantum dot in a GaN nanowire. *Nature Comm.* **2013**, *4*, 1675.

(21) Kremling, K.; Christian, T.; Dartsch, H.; Figge, S.; Höfling, S.; Worschech, L.; Kruse, C.; Hommel, D.; Forchel, A. Single photon emission from InGaN/GaN quantum dots up to 50 K. *Appl. Phys. Lett.* **2012**, *100*, 061115.

(22) Kim, J.- H.; Ko, Y.- H.; Gong, S.- H.; Ko, S.- M.; Cho, Y.- H. Ultrafast single photon emitting quantum photonic structures based on a nano-obelisk. *Sci. Rep.* **2013**, *3*, 2150.

(23) Jarjour, A. F.; Taylor, R. A.; Oliver, R. A.; Kappers, M. J.; Humphreys, C. J.; Tahraoui, A. Cavity-enhanced blue single-photon emission from a single InGaN/GaN quantum dot. *Appl. Phys. Lett.* **2007**, *91*, 052101.

(24) Pal, J.; Tse, G.; Haxha, V.; Migliorato, M. A.; Tomić, S. Second-order piezoelectricity in wurtzite III-N semiconductors. *Phys. Rev. B* **2011**, *84*, 085211.

(25) Avron, J. E.; Bisker, G.; Gershoni, D.; Lindner, N. H.; Meirom, E. A.; Warburton, R. J. Entanglement on Demand through Time Reordering. *Phys. Rev. Lett.* **2008**, *100*, 120501.

(26) Akopian, N.; Lindner, N. H.; Poem, E.; Berlatzky, Y.; Avron, J.; Gershoni, D.; Gerardot, B. D.; Petroff, P. M. Entangled photon pairs from semiconductor quantum dots. *Phys. Rev. Lett.* **2006**, *96*, 130501.

(27) Juska, G.; Dimastrodonato, V.; Mereni, L. O.; Gocalinska, A.; Pelucchi, E. Towards quantum-dot arrays of entangled photon emitters. *Nat. Photonics* **2013**, *7*, 527.

(28) Reimer, M. E.; Dalacu, D.; Poole, P. J.; Williams, R. L. Biexciton binding energy control in site-selected quantum dots. *J. Phys.: Conf. Ser.* **2010**, *210*, 012019.

(29) Reimer, M. E.; van Kouwen, M. P.; Hidma, A. W.; van Weert, M. H. M.; Bakkers, E. P. A. M.; Kouwenhoven, L. P.; Zwiller, V. Electric Field Induced Removal of the Biexciton Binding Energy in a Single Quantum Dot. *Nano Lett.* **2011**, *11*, 645−650.

(30) Andreev, A. D.; O'Reilly, E. P. Optical transitions and radiative lifetime in GaN/AlN self-organized quantum dots. *Appl. Phys. Lett.* **2001**, *79*, 521−523.

(31) Santori, C.; Götzinger, S.; Yamamoto, Y.; Kako, S.; Hoshino, K.; Arakawa, Y. Photon correlation studies of single GaN quantum dots. *Appl. Phys. Lett.* **2005**, *87*, 051916.

(32) De Rinaldis, S.; D'Amico, I.; Rossi, F. Exciton-exciton interaction engineering in coupled GaN quantum dots. *Appl. Phys. Lett.* **2002**, *81*, 4236−4238.

(33) Winkelnkemper, M.; Schliwa, A.; Bimberg, D. Interrelation of structural and electronic properties in $In_xGa_{1-x}N$/GaN quantum dots using an eight-band **k·p** model. *Phys. Rev. B* **2006**, *74*, 155322.

(34) Chuang, S. L.; Chang, C. S. **k·p** method for strained wurtzite semiconductors. *Phys. Rev. B* **1996**, *54*, 2491−2504.

(35) Löwdin, P.-O. Quantum Theory of Many-Particle Systems. I. Physical Interpretations by Means of Density Matrices, Natural Spin-Orbitals, and Convergence Problems in the Method of Configurational Interaction. *Phys. Rev.* **1955**, *97*, 1474−1489.

DOI: 10.1021/acsphotonics.5b00159
ACS Photonics 2015, 2, 958−963

(36) Vukmirovć, N.; Tomić, S. Plane wave methodology for single quantum dot electronic structure calculations. *J. Appl. Phys.* **2008**, *103*, 103718.
(37) Makov, G.; Payne, M. C. Periodic boundary conditions in ab initio calculations. *Phys. Rev. B* **1995**, *51*, 4014−4022.
(38) Tomić, S.; Sunderland, A. G.; Bush, I. J. Parallel multi-band **k·p** code for electronic structure of zinc blend semiconductor quantum dots. *J. Mater. Chem.* **2006**, *16*, 1963−1972.
(39) Ko, Y.-H.; Kim, J.-H.; Jin, L.-H.; Ko, S.-M.; Kwon, B.-J.; Kim, J.; Kim, T.; Cho, Y.-H. Electrically Driven Quantum Dot/Wire/Well Hybrid Light-Emitting Diodes. *Adv. Mater.* **2011**, *23*, 5364−5369.
(40) Lazić, S.; Chernysheva, E.; Gačević, Ž.; Garcia-Lepetit, N.; van der Meulen, H. P.; and Muller, M.; Bertram, F.; Veit, P.; Christen, J.; Torres-Pardo, A.; Gonzalez Calbet, J. M.; Calleja, E.; Calleja, J. M. Ordered arrays of InGaN/GaN dot-in-a-wire nanostructures as single photon emitters. *Proc. SPIE* **2015**, *9363*, 93630U.
(41) Birowosuto, M. D.; Sumikura, H.; Matsuo, S.; Taniyama, H.; van Veldhoven, P. J.; Nötzel, R.; Notomi, M. Fast Purcell-enhanced single photon source in 1,550-nm telecom band from a resonant quantum dot-cavity coupling. *Sci. Rep.* **2012**, *2*, 321.
(42) Claudon, J.; Bleuse, J.; Malik, N. S.; Bazin, M.; Jaffrennou, P.; Gregersen, N.; Sauvan, C.; Lalanne, P.; Gerard, J.-M. A highly efficient single-photon source based on a quantum dot in a photonic nanowire. *Nat. Photonics* **2010**, *4*, 174−177.
(43) Matthiesen, C.; Vamivakas, A. N.; Atatüre, M. Subnatural Linewidth Single Photons from a Quantum Dot. *Phys. Rev. Lett.* **2012**, *108*, 093602.

DOI: 10.1021/acsphotonics.5b00159
ACS Photonics 2015, 2, 958−963